OXFORD

Journal of Geophysics and Engineering

Journal of Geophysics and Engineering (2020) **17**, 484–492 doi:10.1093/jge/gxaa007

Prediction of hydrocarbon reservoirs within coal-bearing formations

Faqi He[1], **Ying Rao**[2,*], **Weihong Wang**[3] **and Yanghua Wang**[4]

[1] Sinopec Northern China Petroleum Bureau, Zhengzhou, Henan 451200, China
[2] State Key Laboratory of Petroleum Resources and Prospecting, China University of Petroleum (Beijing), Changping District, Beijing 102249, China
[3] Bohai-Rim Research Institute of Energy, Northeast Petroleum University, Qinhuangdao, Hebei 066004, China
[4] Centre for Reservoir Geophysics, Resource Geophysics Academy, Imperial College London, South Kensington, London SW7 2BP, UK

*Corresponding author: Ying Rao. E-mail: raoying@cup.edu.cn

Received 16 December 2019, revised 15 January 2020
Accepted for publication 24 January 2020

Abstract

This paper presents a case study on the prediction of hydrocarbon reservoirs within coal-bearing formations of the Upper Palaeozoic. The target reservoirs are low-permeability low-pressure tight-sandstone reservoirs in the Daniudi Gas Field, Ordos Basin, China. The prime difficulty in reservoir prediction is caused by the interbedding coal seams within the formations, which generate low-frequency strong-amplitude reflections in seismic profiles. To tackle this difficulty, first, we undertook a careful analysis regarding the stratigraphy and lithology of these coal-bearing formations within the study area. Then, we conducted a geostatistical inversion using 3D seismic data and obtained reservoir parameters including seismic impedance, gamma ray, porosity and density. Finally, we carried out a reservoir prediction in the coal-bearing formations, based on the reservoir parameters obtained from geostatistical inversion and combined with petrophysical analysis results. The prediction result is accurately matched with the actual gas-test data for the targeted four segments of the coal-bearing formations.

Keywords: geostatistical inversion, reservoir prediction, clastic reservoir, coal-bearing formations, Ordos Basin

1. Introduction

This is a case history paper, focusing on the prediction of hydrocarbon reservoirs within coal-bearing formations of the Upper Palaeozoic. The study area is in the Daniudi Gas Field, Ordos Basin, North China block (Şengör & Natal'in 1996; Guo *et al.* 2001; Wang *et al.* 2005).

The Daniudi Gas Field is tectonically on the nose-like Taba-Temple uplift, in the northeastern part of the Iginholo-Shaanxi slope (figure 1). It is approximately 2000 km^2, with a square shape spatially (marked in red, figure 1). It is located on the top of the slope of the ancient weathering crust; hence, it has the right development conditions for hydrocarbon reservoirs. However, the gas reservoir in this gas field is a low-permeability low-pressure tight-sandstone reservoir (Gan *et al.* 2009; Hou & Liu 2012; Yang *et al.* 2016). The average permeability of reservoirs is about 0.54×10^{-3} μm^2, and the pressure coefficient of the gas reservoirs is 0.8–1.0. An average single-well production rate is as low as 0.5×10^4 m^3 per day. It is indeed a marginal gas field, if measured in terms of economic prospecting.

There were two coal-bearing formations in the Upper Palaeozoic: the Shanxi (S) Formation of the Permian age and the Taiyuan (T) Formation of the Carboniferous age. These

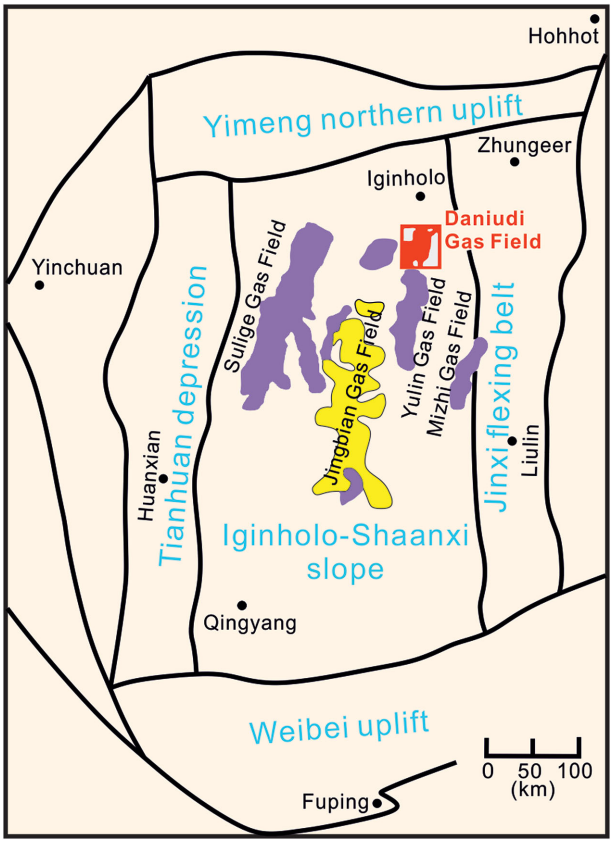

Figure 1. Daniudi Gas Field (in red) is tectonically in the northeastern part of the Iginholo-Shaanxi slope, Ordos Basin, North China block. The Iginholo-Shaanxi slope is surrounded by the Yimeng northern uplift in the north, the Weibei uplift in the south, the Tianhuan depression in the west and the Jinxi flexing belt in the east. In the immediate south side of the Daniudi Gas Field, there are several gas fields that are spread sequentially from west to east: Sulige Gas Field, Jingbian Gas Field, Yulin Gas Field and Mizhi Gas Field.

two formations may further be divided into four segments, S2, S1, T2 and T1, from the top to the bottom. All these four segments in the Daniudi Gas Field have good reservoir development conditions and all have industrial-scale gas flow potential (Zhang *et al.* 2011).

Within these coal-bearing formations, coal seams and sand layers lay on top of each other. Such overlaying and interbedding characteristics make both reservoir prediction and fluid identification very difficult. This is especially so when a target reservoir is immediately above or below a coal seam, and the application of seismic information could be very difficult (Wang 2012). This is because of the large differential in seismic impedance between a coal seam and a non-coal layer, which generates a strong reflection on the seismic profile (figure 2). Such a strong reflection of the coal seam will submerge the effective information and thus cause difficulty in the prediction of reservoirs and the fluid contents within the coal-bearing strata.

For instance, the sedimentary facies map (figure 3) indicates that the S1 segment of the Permian is densely covered by the distributary channels and therefore also by the well-deposited sand bodies. On the seismic profile (figure 2), the S1 segment corresponds to the wave peak (indicated by arrows) and the upper edge of the waveform. Influenced by the low-frequency strong-amplitude reflection of coal seams, the seismic resolution is low, and the accuracy of reservoir prediction within the S1 segment is low. As a consequence, the way to conduct hydrocarbon reservoir prediction through coal-bearing formations is an urgent problem that needs to be resolved in reservoir geophysics.

In this study, we undertake stratigraphic and lithologic analyses of the Upper Palaeozoic formations in the study area, and a petrophysical analysis of the logging data within

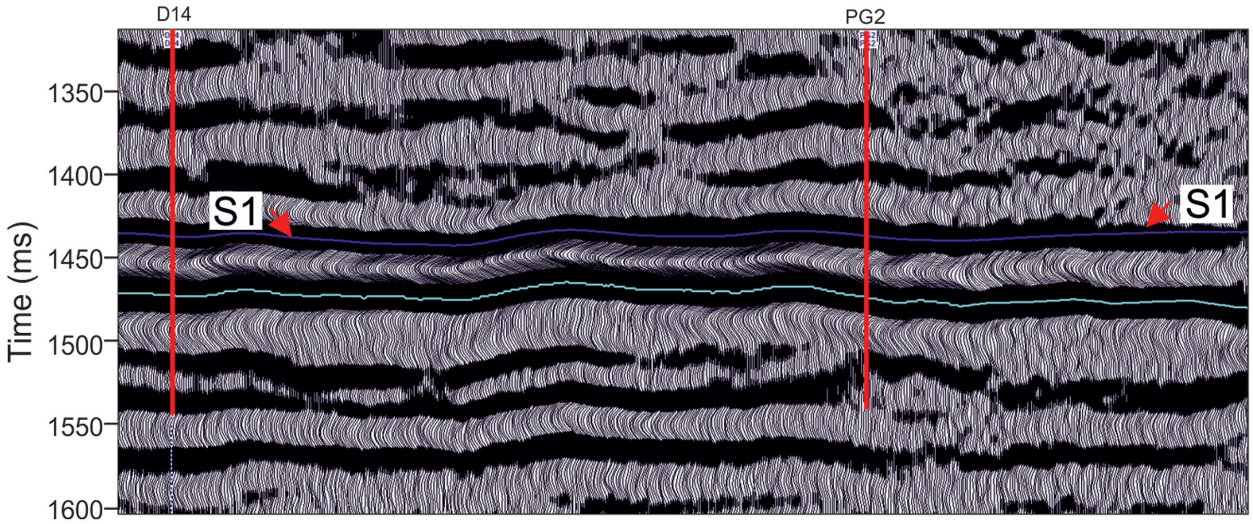

Figure 2. Seismic profile of the Daniudi Gas Field, which shows that the S1 segment within the Shanxi Formation corresponds to the wave peak indicated by red arrows and the upper edge.

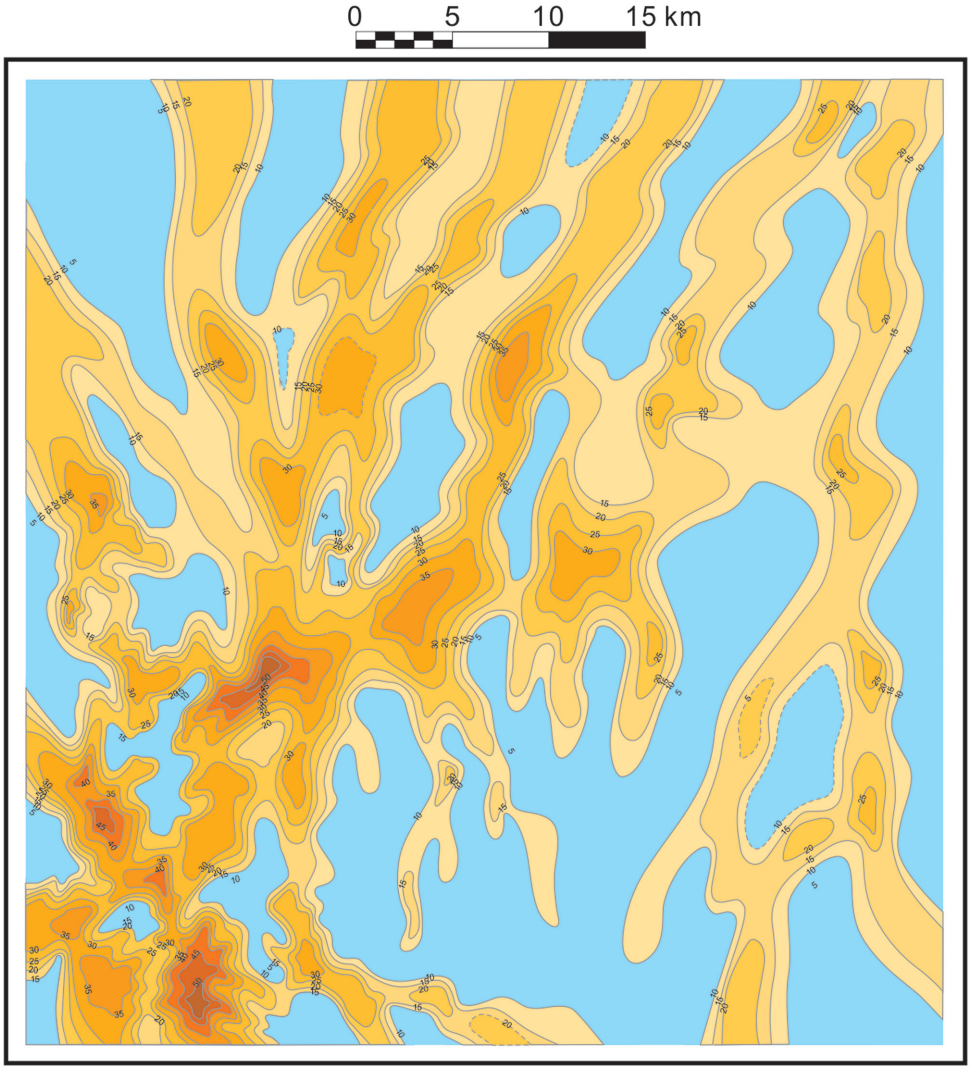

Figure 3. Sedimentary facies of the S1 segment, Daniudi Gas Field. The S1 segment is densely covered by the distributary channels, and therefore was also covered by well-deposited sand bodies. The contours show the thickness of sand deposition.

the clastic reservoirs (Liu *et al.* 2019). Then, we carry out 3D seismic inversion using the geostatistical method to obtain reservoir parameters including seismic impedance, gamma ray, porosity and density. Finally, we conduct reservoir prediction for the four segments sequentially within coal-bearing formations.

2. Lithology of coal-bearing formations

In this study, we select the well E8 area as the target area, since it is in the central part of the gas field. Table 1 lists the stratigraphic and lithologic properties of the Upper Palaeozoic that were encountered by well E8. This well was drilled in October 1992, and it is located at the Hanging-well Ridge, Maogettu Brigade of Taigemiao Town, Iginholo, Inner Mongolia. The coordinates are $x = 4\,321\,567.7$ m, $y = 19\,388\,132.1$ m, and $h = 1333.6$ m. Table 1 also lists the depths and the thicknesses of four segments S2, S1, T2 and T1.

The focus of the study is on the two coal-bearing formations, the S and T Formations of the Upper Palaeozoic. The lithology of S Formation is composed of mainly grey medium-coarse sandstone, glutenite, conglomerate, interbedded with black, dark-grey mudstone and black carbonaceous mudstone. The lower part of the S formation contains coal seams and coal sheets. The lithology of the T Formation is mainly dark-grey, black mudstone, carbonaceous mudstone, and coal seams that are interbedded with grey-white medium-coarse sandstone and partially intercalated limestone lenses.

In addition, this gas field also includes the overlying Lower Shihezi Formation and the underlying Ordovician carbonate weathering in the Lower Palaeozoic. The lithology of the Lower Shihezi Formation is mainly light-grey, grey-white glutenite, pebbly coarse sandstone and medium-coarse sandstone, which are interbedding with grey, brown mudstone. The Benxi Formation of the Carboniferous at the

Table 1. Stratigraphic and lithologic properties of the Upper Palaeozoic, encountered by well E8 in the Daniudi Gas Field.

Stratum system			Drilling depth	
System (era)	Series	Formation	[thickness] (m)	Lithology
Upper Palaeozoic	Permian	Lower Shihezi Formation	2645.0 [85.5]	Grey-white, grey-purple glutenite, pebbly coarse sandstone, pebbly sandstone, medium-fine sandstone, argillaceous siltstone, interbedded with grey-purple, grey-black, grey, black silty mudstone, and mudstone. These interbeds have a similar thickness.
		Shanxi Formation	2706.0 [61.0]	Upper part: greyish white, light-grey pebbly medium-coarse sandstone, gravel medium sandstone, medium-silty sandstone, argillaceous siltstone, interbedding with dark-grey, greyish black silty mudstone, mudstone. These interbeds have an unequal thickness. Lower part: mudstone interbedded with medium sandstone, argillaceous siltstone. These interbeds have a similar thickness.
	Carboniferous	Taiyuan Formation	2788.5 [82.5]	Greyish white, light-grey, medium, silty sandstone, argillaceous siltstone, interbedding with dark-grey, greyish black silty mudstone, mudstone. These interbeds have a similar thickness. Sandwiching six coal seams and three layers of carbonaceous mudstone.
		Benxi Formation	2800.3 [11.8]	Light-grey, grey, dark-grey, grey-black mudstone, aluminous mudstone, interbedding with light-grey, grey, dark-grey, greyish black pyrite-bearing mudstone, muddy pyritic rock, and pyrite-bearing aluminous mudstone. These interbeds have a similar thickness. The top is greyish white fine sandstone, and the part is aluminous earthy mudstone.
Lower Palaeozoic	Ordovician	Upper Majiagou Formation	3153.0 [352.7]	Dark-grey, greyish white, black-grey, grey-black dolomite, mud-bearing dolomite, argillaceous dolomite, lime-bearing dolomite, mud-lime-bearing dolomite, lime-bearing mud-dolomite, lime-dolomite, and mud-bearing lime-dolomite, interbedded with dark-grey, black-grey mud-bearing limestone, dolomite-bearing limestone, mud-bearing dolomitic limestone, dolomitic limestone, limestone. These interbeds have unequal thickness. The top sandwiches a layer of black-grey silty-sand-bearing dolomitic mudstone.

bottom of the Upper Palaeozoic is only 11.8 m in thickness, while the T Formation is 82.5 m in thickness, and interbedded with six coal seams and three layers of carbonaceous mudstone.

Colour is one of the important macroscopic features of sedimentary rocks and this is closely related to the composition of rocks and their depositional environment. Therefore, the original colour of the rock is a good reflection of the physical and chemical conditions of the water body when the rock was formed. In general, the colour was light and oxidized when the rock was formed in a shallow water or oxidation environment, and the colour was dark when the rock was formed in a deep water or redox environment.

3. Petrophysical properties of coal-bearing formations

We carry out the petrophysical analysis based on cross-plots (Chatterjee & Paul 2012) between the gamma-ray value (the vertical axis, figure 4) and other petrophysical parameters, including the P-wave velocity, P-wave impedance, density and compensated neutron logging (CNL) porosity (the horizontal axis). Then, according to the known gas saturation (colour bar in figure 4), we delineate the upper and lower limits of each parameter in the well E8 area.

Figure 4 is a clastic petrophysical analysis of the S and T Formations. The cross-plotting results show that the gamma-ray value of the clastic gas reservoir in the well E8 area is less than 85 gAPI. The density is between 2.1 and 2.7 g · cm^{-3}, but the low density (2.1–2.4 g · cm^{-3}) may be a coal seam, and the relatively high density (2.4–2.7 g · cm^{-3}) may be a gas-bearing layer.

The fourth panel in figure 4 is a cross-plot of the gamma ray value and the CNL porosity. The CNL value measures the hydrogen content of the formation and its value can be approximated as an estimate of formation porosity. The limestone has a CNL value of 0 and the water has a CNL value of 100. For the sandstone, when the porosity is high, the CNL value is also high, and when the porosity is low, the CNL value is also low.

The CNL response to an oil layer is not so obvious. However, for a gas layer, the CNL value will be lower than the

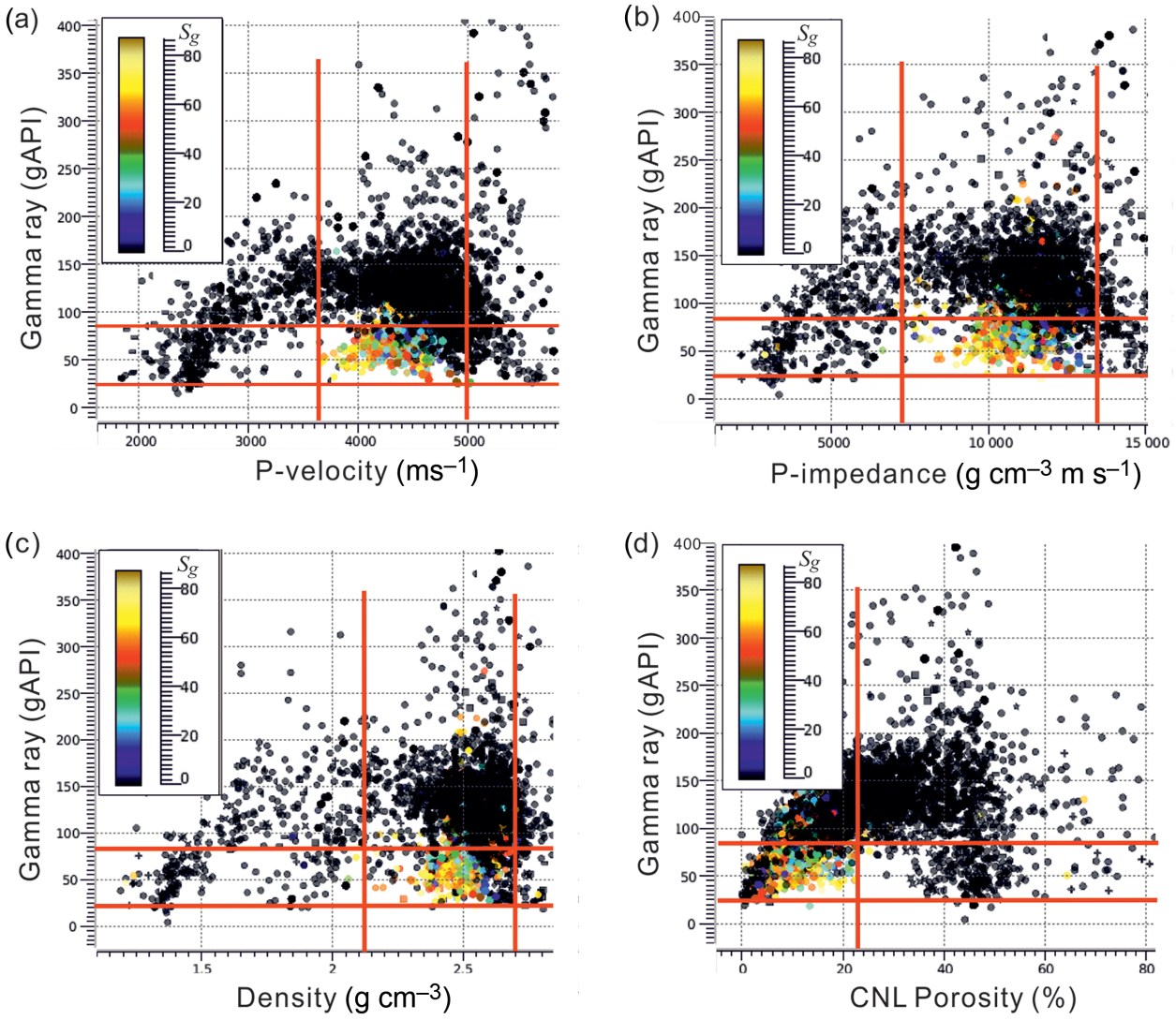

Figure 4. Petrophysical analysis of coal-bearing formations (S formation and T formation). The colour bar is the gas saturation (S_g).

actual porosity. The larger the volume of gas content of the formation, the lower the CNL value. The fourth panel in figure 4 clearly shows that the CNL value of the clastic formation in the well E8 area is less than 22%. The CNL value for commercial gas flows is generally less than 12%, and sometimes it is as low as 3%, or even less.

Based on the clastic petrophysical analysis here, which was compared against the gas saturation (colour sample), a list of the upper and lower limits of the gas content indication for each parameter is presented in Table 2.

4. Geostatistical inversion

We perform geostatistical inversion of 3D seismic data to obtain four reservoir parameters including P-wave impedance, density, gamma value and porosity (Bosh *et al.* 2010). In the seismic inversion, we first use a sparse inversion method to obtain a low-wavenumber background model for P-wave impedance, and then use a geostatistical inversion method to invert for the four reservoir parameters simultaneously.

The parameters of the sparse inversion method include: P-wave impedance uncertainty (=0.02), signal-to-noise ratio (=12), the Lp norm of seismic data residual ($P = 0.7$) and the cut-off frequency (=9 Hz). The geostatistical inversion method we used is the Gaussian collocated cosimulation (Soares 2001; Nunes *et al.* 2017).

Figure 5 shows the coverage of the well-E8 3D seismic data in the Daniudi Gas Field. The 3D seismic data cube covers a 195 km^2 area of the 3D seismic survey, and well E8 (marked in red colour) is slightly northerly in the centre. There is an arbitrarily selected cross-well line passing through 10 wells: D12-66, DPH-114-D, D12-8, DPS-18-D, E10, D10-17, D-8, D41, PG6-D and D96. Two green stars indicate the two wells annotated in the seismic profile shown in figure 2.

Table 2. Petrophysical analysis of coal-bearing strata.

Well logging data	Lower limits	Upper limits
Gamma ray (gAPI)	>25	<85
P-wave velocity ($m \cdot s^{-1}$)	>3600	<5000
P-wave impedance ($g \cdot cm^{-3}$ $m \cdot s^{-1}$)	>7200	<13 600
Density ($g \cdot cm^{-3}$)	>2.12	<2.72
CNL (porosity, %)		<22

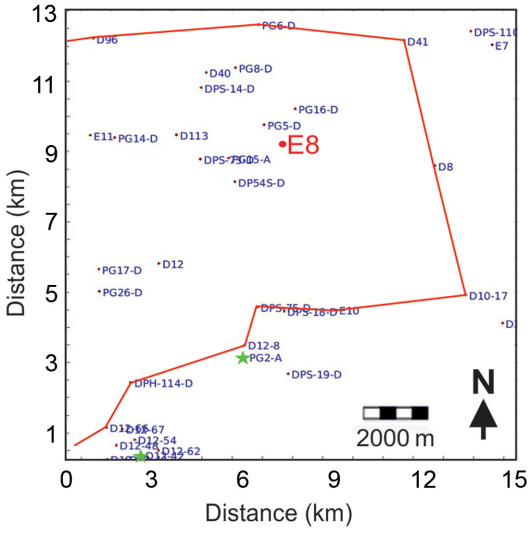

Figure 5. The coverage of the well-E8 3D seismic data in the Daniudi Gas Field. Well E8 (marked in red) is slightly more to the north in the centre. There is an arbitrarily selected seismic line connecting 10 wells. Two green stars indicate the two wells annotated in the seismic profile shown in figure 2.

Figure 6 displays the geostatistical inversion results following this cross-well line. The inversion results reveal that the P-wave impedance and density of the Ordovician carbonate formation are significantly higher than the overlying clastic formation. The gamma-ray value of the Ordovician carbonate formation is significantly lower than that of the overlying clastic formation. In the inversion results, it is abundantly clear to see that the coal seams have the characteristics of low impedance, low density and high gamma-ray value. But the correspondence between the porosity and either the clastic or carbonate rocks is not obvious (Liu *et al.* 2018; Li *et al.* 2019).

5. Reservoir prediction of coal-bearing formations

For coal-bearing formations in the Upper Palaeozoic, we conduct reservoir prediction interactively, based on the cross-plot of the gamma ray and density values. It is noteworthy that we use the density rather than the porosity in the prediction of these clastic reservoirs. We perform in this manner to avoid the effect of coal seams and to achieve that by setting the density to be greater than 2.4% as a threshold. Meanwhile, we set the gamma-ray value to be less than 85 gAPI.

Figure 7 shows the results of the reservoir prediction for the S2, S1, T2 and T1 segments, respectively. The colour scale indicates the reservoir thickness, which is quantified in terms of seismic time in units of ms.

The S2 segment is the sub-facies of the braided river delta plain. The sedimentary microfacies are the distributary channels and depressions and swamps between channels. In this area, the S2 segment is well-developed with respect to the distributary channels, which exhibit the characteristics of extending from north to south and of multi-level distributaries and convergence. The thickness of sand body is 4.5 m on average. The sand body formed by the sedimentary microfacies of the distributary channels has a large thickness, a coarse grain size and a good sorting property, so the sandstone has a good porosity and permeability and is the most favourable reservoir layer (Chen & Wang 2010). The sand body that formed at the edge of river channels is thin, fine in grain size, poor in physical properties and weak in its ability to store natural gas. The prediction result in figure 7a shows that the sand body in some individual depressions and swamps might reach a thickness of 15 ms (about 30 m).

The S2 segment discussed basically contains no coal seams, while the S1 segment is a coal-bearing stratum. Although the layer thickness of the S1 segment is about 50–70 m on average, and it is relatively large, the sandstone layers are much more dense vertically and the grain size is relatively coarse (Dong *et al.* 2009) because of the presence of coal seams in the S1 segment. The effective reservoir thickness within the S1 segment is relatively small, as shown in figure 7b, compared to the effective reservoir thickness of the S2 segment.

The sediment of the T Formation is mainly composed of a barrier-type coastal facies. This coastal facies is characterized by a set of interbedded shelf and paralic sediments, including lake-marsh and littoral mudstones, carbonaceous mudstones, limestones, coal seams and coastal-littoral sandstones with varying degrees of development. A rhythmic deposition of marine carbonate-mudstone-thin coal seam is a typical representative of the middle-late sedimentation of the T Formation. Tidal flats, lagoons and barrier islands are sedimentary facies that developed in the T Formation. Sedimentary microfacies mainly include barrier sand dams, sand flats and mixed rafts. The reservoir rock types are mainly composed of pebbly coarse sandstone, coarse sandstone, medium sandstone, fine sandstone and siltstone. The reservoir pore type is mainly secondary, the throat is mainly fine and the pore throat connectivity is medium.

The rock type of the T2 segment is mainly medium-coarse quartz sandstones. The volume fraction of quartz in the

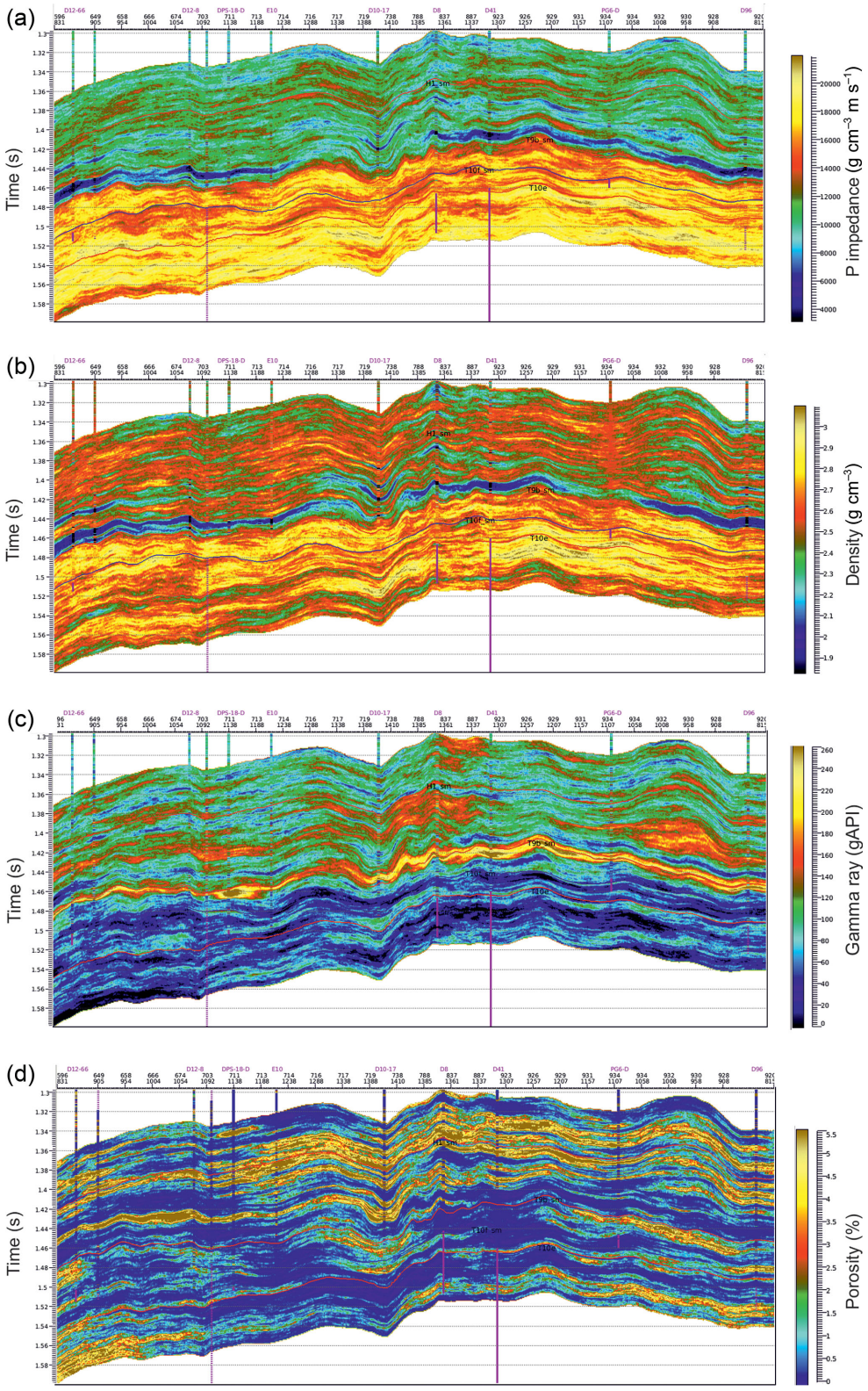

Figure 6. Cross-well profile of the 3D seismic inversion results in the well E8 area. (a) P-wave impedance. (b) Density. (c) Gamma-ray value. (d) Porosity.

sandstone crumb structure reaches 71–98% and the average debris is 13.4%. The sorting of granule rounding is generally fine and good, and the rounding is mainly in a round form. The cementing type is mainly regenerative pores and primary pores. The cements contain authigenic quartz, calcite, dolomite and a small amount of siderite.

The rock type of the T1 segment is mainly coarse-grained quartz sandstone. Quartz volume fraction is 92.3–99.8%, and

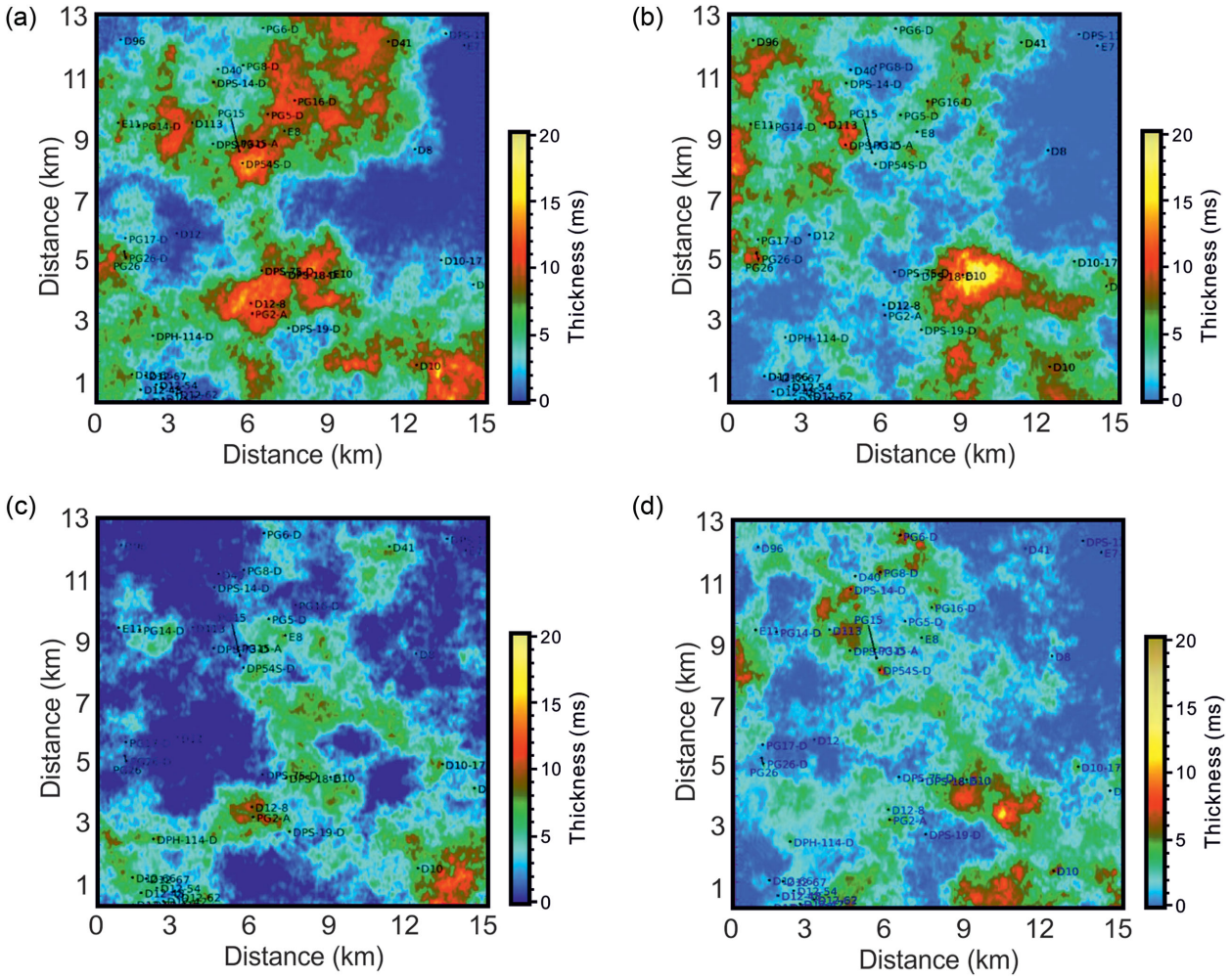

Figure 7. Reservoir prediction of S2 segment in the well E8 area. (a) Reservoir prediction of S2 segment. (b) Reservoir prediction of the S1 segment. (c) Reservoir prediction of the T2 segment. (d) Reservoir prediction of the T1 segment. The colour scale is the reservoir thickness (in ms).

the debris is 0–6.5% with almost no feldspar. The granule sorting is between medium and good, and the rounding is dominated by a sub-angular shape. The cementing type is mainly regenerative pores and primary pores, and there is a small number of compaction pores.

In the T2 segment, the class II gas reservoirs (medium-yield gas reservoirs, with unobstructed flow greater than 1.0×10^4 m^3 per day and less than 5.0×10^4 m^3 per day) had the widest distribution and were mainly developed in the middle of the sand dams. Class III gas reservoirs (low-yield gas reservoirs, with unobstructed flow less than 1.0×10^4 m^3 per day and greater than 0.5×10^4 m^3 per day) were secondarily developed on the edge of sand dams. Class I gas reservoirs (high-yield gas reservoirs with unobstructed flow above 5.0×10^4 m^3 per day) were distributed in the right centre of the barrier sand dams.

The class I gas reservoirs in the T2 segment were more widely distributed than the T1 segment. The lithology of these areas in a large portion of the T2 segment is the coarse and coarser sandstone. These areas in the T2 segment generally have a good physical property, a large thickness of sandstone and fewer interbeds. However, the reservoir predictions show that the reservoir thickness of both T2 and T1 segments within the Taiyuan Formation is relatively thin (figures 7c and 7d).

6. Conclusion

We have conducted the stratigraphic and lithologic analyses of the coal-bearing formations and the petrophysical analysis of the logging data, and delineated the upper and lower limits of each petrophysical parameter according to the known gas saturation. The cross-plotting results show that the clastic gas reservoirs in this area have the gamma-ray value between 25 and 85 gAPI, a density value between 2.1 and 2.7 g · cm^{-3} and CNL porosity value below 22%.

Geostatistical inversion of the 3D seismic data has produced elastic and reservoir parameters including P-wave

impedance, density, gamma-ray value and porosity. The inversion results show that the P-wave impedance and density of the overlying clastic formations are significantly lower than those of the underlying Ordovician carbonate rock. The gamma ray value of the overlying clastic formations is significantly higher than that of the underlying Ordovician carbonate. The clastic formations have the obvious characteristics of low impedance, low density and high gamma-ray value. The correspondence between porosity and either clastic or carbonate rocks is not obvious.

In this study, we have set a threshold value for the density to effectively exclude the interference of coal seams. We have compared the reservoir prediction result with the geological characteristics such as the sedimentary facies and reservoir types, and found that the prediction result is finally matched with the actual gas-test data for each segment of the coal-bearing formations.

Acknowledgements

The authors are grateful to the National Natural Science Foundation of China (grant nos. 41974116, 41974118 and U19B6003), the Science Foundation of China University of Petroleum (Beijing) (grant no. 2462018BJC001) and the sponsors of the Centre for Reservoir Geophysics, Resource Geophysics Academy, Imperial College London, for supporting this research.

Conflict of interest statement. None declared.

References

Bosh, M., Mukerji, T. & Gonzalez, E.F., 2010. Seismic inversion for reservoir properties combining statistical rock physics and geostatistics: a review, *Geophysics*, **75**, 75A165–75A176.

Chatterjee, R. & Paul, S., 2012. Application of cross-plotting techniques for delineation of coal and non-coal litho-units from well logs, *Geomaterials*, **2**, 94–104.

Chen, Z.Y. & Wang, G.Q., 2010. Sandstone combination types and genetic models of the Shanxi Formation in the Daniudi Gas Field, Ordos Basin, *Oil and Gas Geology*, **31**, 632–639 (in Chinese).

Dong, Z.X., Shen, Z.G., He, G.X. & Liu, Z.Q., 2009. Relationship between sedimentary microfacies and reservoir in the Shan-1 segment of Daniudi Gas Field, Ordos Basin, *Oil and Gas Geology*, **30**, 162–167 (in Chinese).

Gan, Q., Xu, D., Tang, J. & Wang, Y., 2009. Seismic resolution enhancement for tight-sand gas reservoir characterization, *Journal of Geophysics and Engineering*, **6**, 21–28.

Guo, F., Fan, W., Wang, Y.-J. & Lin, G., 2001. Late Mesozoic mafic intrusive complexes in North China block: constraints on the nature of subcontinental lithospheric mantle, *Physics and Chemistry of the Earth A: Solid Earth and Geodesy*, **26**, 771–795.

Hou, R.Y. & Liu, Z.Q., 2012. Evaluation and development countermeasures for tight-sand low-permeability reservoirs in Daniudi Gas Field, Ordos Basin, *Oil and Gas Geology*, **33**, 118–128 (in Chinese).

Li, X., Li, Q. & Shen, H., 2019. Rayleigh-wave imaging of the loess sediments in the southern margin of the Ordos Basin by improved frequency–wavenumber transform, *Journal of Geophysics and Engineering*, **16**, 77–84.

Liu, M., Xie, R., Li, C., Li, X., Jin, G. & Guo, J., 2018. Determining the segmentation point for calculating the fractal dimension from mercury injection capillary pressure curves in tight sandstone, *Journal of Geophysics and Engineering*, **15**, 1350–1362.

Liu, W., Zhang, G., Cao, J., Zhang, J. & Yu, G., 2019. Combined petrophysics and 3D seismic attributes to predict shale reservoirs favourable areas, *Journal of Geophysics and Engineering*, **16**, 974–991.

Nunes, R., Soares, A., Azevedo, L. & Pereira, P., 2017. Geostatistical seismic inversion with direct sequential simulation and co-simulation with multi-local distribution functions, *Mathematical Geosciences*, **49**, 583–601.

Şengör, A.M.C. & Natal'in, B.A., 1996. Paleotectonics of Asia: fragments of a synthesis, in *The Tectonic Evolution of Asia*, pp. 486–640, eds Yin A. & Harrison T.M., Cambridge University Press, Cambridge, UK.

Soares, A., 2001. Direct sequential simulation and co-simulation, *Mathematical Geology*, **33**, 911–926.

Wang, Y., 2012. Reservoir characterization based on seismic spectral variations, *Geophysics*, **77**, M89–M95.

Wang, Y., Houseman, G.A., Lin, G., Guo, F., Wang, Y.J., Fan, W.M. & Chang, X., 2005. Mesozoic lithospheric deformation in the North China block: numerical simulation of evolution from orogenic belt to extensional basin system, *Tectonophysics*, **405**, 47–63.

Yang, Z., He, S., Guo, X., Li, Q., Chen, Z. & Zhao, Y., 2016. Formation of low permeability reservoirs and gas accumulation process in the Daniudi Gas Field, Northeast Ordos Basin, China, *Marine and Petroleum Geology*, **70**, 222–236.

Zhang, G.Q., Chen, S.W. & Guo, S.Y., 2011. Sedimentary facies of the Shanxi Formation of the Daniudi Gas Field, Northeastern Ordos basin, *Oil and Gas Geology*, **32**, 388–396 (in Chinese).